Profiles of Optical Extinction Coefficients Calculated from Droplet Spectra Observed in Marine Stratus Cloud Layers

V. RAY NOONKESTER

Ocean and Atmospheric Sciences Division, Naval Ocean Systems Center, San Diego, CA 92152

(Manuscript received 6 August 1984, in final form 13 February 1985)

ABSTRACT

Airborne measurements of droplet spectra $n(r)$ where r is droplet radius were made in stratus cloud layers over the ocean 130 km southwest of San Diego. Optical extinction coefficients σ_e were calculated at selected wavelengths (λ = 0.53, 3.75 and 10.59 μm) from these $n(r)$ and were used to construct average vertical profiles of σ_e between 200 m above cloud base to 250 m below cloud base. An approximation to σ_e, a power function of the liquid water content w, was found to be superior compared with approximations involving linear functions of w or the cross-section area. The horizontal variability of σ_e in the clouds was examined. The average horizontal scale size of σ_e was estimated to be 3 km and the horizontal measuring distance required to obtain values of σ_e with a relative accuracy of 10% was found to be in excess of 30 km.

1. Introduction

Improvements in atmospheric general circulation models require more complete knowledge on the spatial distribution of clouds and on their radiative properties than presently available (Herman *et al.*, 1980). The capacity of clouds to reflect, absorb, transmit and emit radiation depends on their geometric features (Davies, 1978), temperature, water vapor content and particularly on the size distribution of the liquid water droplets usually described by the spectrum $n(r)$ where r is droplet radius. Lack of data on the distribution of $n(r)$ within various cloud types poses the most serious limitation on studies of the effects of clouds on the atmospheric radiation balance (Stephens, 1978a). This sparsity of data has prompted some investigators to assume a homogeneous distribution of $n(r)$ throughout a cloud (e.g., Herman *et al.*, 1980) although the vertical variation of $n(r)$ has been found to have an important control on the radiative properties of clouds (e.g., Slingo *et al.*, 1982a). Horizontal variations in $n(r)$ in clouds (Noonkester, 1984) may also pose problems in characterizing the radiative properties of clouds (e.g., Slingo *et al.*, 1982b).

Although the controlling optical properties of cloud droplets are determined from Mie-theory calculations, these calculations are considered to be too cumbersome when used in atmospheric radiation models (Stephens, 1978b; Slingo and Schrecker, 1982). Recent parameterization schemes avoiding Mie-theory calculations have encouraged the use of simple formulations involving the liquid water content of the droplets w and the effective droplet radius r_e to specify the single-scatter, volume, extinction coefficient σ_e by droplets (Stephens, 1978b; Slingo and Schrecker, 1982). Thus, when the vertical variation of representative $n(r)$ in a cloud is known, w and r_e can be calculated and used to specify σ_e as a function of elevation. Although specification of σ_e as a function of depth in the cloud does not provide complete parameterization of all required optical properties, such specification appears to be critical in contemporary parameterization schemes.

Relatively high resolution measurements of the vertical variations of $n(r)$ in eight marine stratus cloud layers were recently described by Noonkester (1984) which indicated that the vertical variations of $n(r)$ were commensurate with the classical growth (Fitzgerald, 1975; Neiburger and Chien, 1960) of droplets in a well mixed layer, in particular, from the surface to cloud base. Arguments were presented to indicate that the data could be divided into stratus layers forming in air masses approximating marine or continental sources. These internally consistent sets of $n(r)$ were used in this paper to obtain σ_e by Mie-theory calculations as a function of distance from the cloud base for the two air masses at wavelengths λ of 0.53, 3.75, and 10.59 μm. Radiation at these discrete wavelengths was selected to represent the visible and near IR region of electromagnetic radiation influencing the atmospheric radiation balance. The utility of approximations to σ_e, given as functions of the cross section area A and w, was determined by comparison with Mie-theory calculations of σ_e. The major purpose of this paper is to present these comparisons.

The measurements of $n(r)$ along two-minute horizontal runs provided data to obtain the horizontal variability and the average scale size of σ_e. Furthermore, the measuring distance required to obtain

values of σ_e with a relative accuracy of 10% was estimated. These data should provide guidance in developing radiation models for and making measurements in marine stratus cloud layers. A more detailed discussion of the measurements is provided by Noonkester (1984), hereinafter called Paper I.

2. Sensors and measurements

Airborne measurements of the droplet spectra $n(r)$ were made as a function of elevation z along two-minute horizontal runs (6.44 km) at 13–16 levels in marine stratus cloud layers 130 km southwest of San Diego, California. The sampling period was 5 and 8 s for z and $n(r)$, respectively. Each 8 s spectra (0.23 μm $\leqslant r \leqslant$ 155 μm), representing 429 m along a run, was obtained by an ASSP-100 and an OAP-200, manufactured by Particle Measuring Systems, Inc. Thus, 24 measurements of elevation and 15 droplet spectra were obtained along each 2-min run. The z's were accurate to ±2–3 m below 700 m and the average standard deviation of z along the runs was 4.7 m.

The temperature and dew point were also measured along each run but the temperature was considered suspect so that the vertical mixing characteristics indicated by the temperature and the relative humidity could not be obtained (details in Paper I).

Measurements were made in horizontally extensive decks of stratus clouds (verified by satellite visual imagery) on three days in May 1981 and five days in August 1981 before 0930 PST each day. Several horizontal runs were made near the visually indistinct cloud bases to obtain good estimates of the vertical gradients of $n(r)$. Figure 1 shows the flight levels for each day of measurement. The average cloud base height (cloud base to be defined) was 452 m and the average cloud thickness was 320 m. Data taken during May and August were concluded to be taken when modified marine and continental air masses were, respectively, present. Data on 29 May and 18 August were selected to represent the two air masses and were examined in detail. These days will hereinafter be referred to as M29 and A18, respectively.

The differences between the measured and true values of the $n(r)$'s are unknown. Based on the collected opinion of many users of PMS spectrometers, Baumgardner and Dye (1983) summarized the status of measurement problems using PMS spectrometers (especially FSSP's) indicating that sizing and concentration errors are inherent in the instruments and that acceptable methods to compensate for the errors are not available. Careful, repeated checking and factory calibrations of the spectrometers used in this study provided increased confidence of proper operation. The number of droplets in the size range measured by the OAP-200 (14.2 μm $\leqslant r \leqslant$ 155 μm) was insufficient to make a significant contribution to any parameter derived from $n(r)$ except sporadically along some runs near the surface.

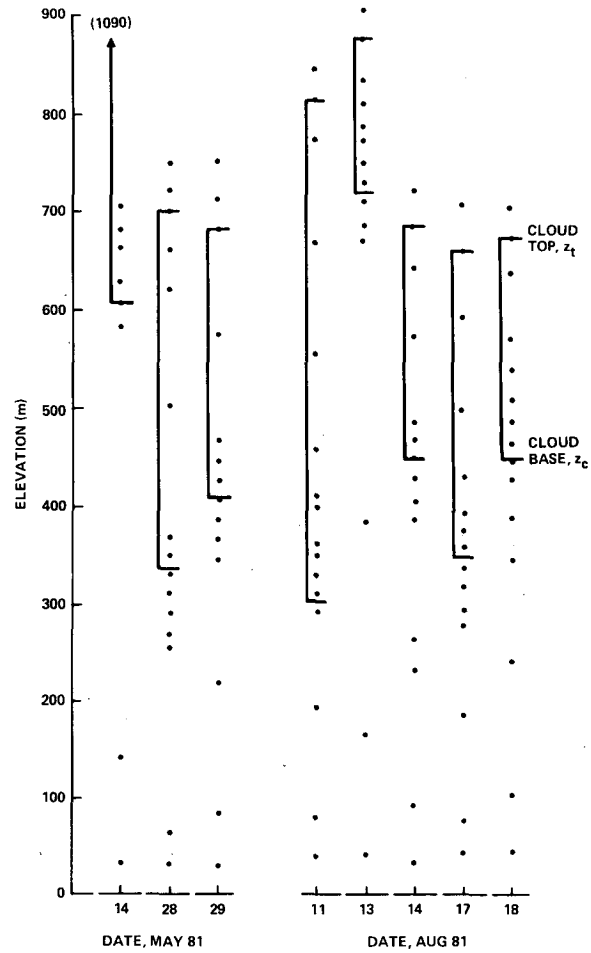

FIG. 1. Elevations of the cloud bases z_c ($\langle w \rangle$ = 0.02 g m^{-3}), the cloud tops z_t and the horizontal runs (dots) by the airborne sensor system.

The spectrometers were constructed to size all particles as spherical droplets having a refractive index of pure water. If the true refractive index of the droplets is other than that of pure water, additional sizing errors are produced. The assumption that the droplets are pure water may be approximately correct for large droplets when small nuclei are involved. Indirect evidence (Paper I) suggests that the nuclei approximated NaCl on M29 and $(NH_4)_2SO_4$ on A18. Many types of nuclei are likely off the coast of California (e.g., Hidy *et al.*, 1974) during strong offshore flow from nearby coastal regions so that sizing errors could be highly variable when fresh continental air masses are sampled. The refractive indices used to calculate σ_e from $n(r)$ may not represent the actual set of nuclei. No other data such as radiometer measurements were taken to aid in the determination of errors in $n(r)$ or σ_e. Thus, there appears to be no method available in this study to

make estimates of the errors in $n(r)$ or any parameter derived from $n(r)$ such as σ_e.

Some data are available to indicate expected differences in $n(r)$ obtained by PMS spectrometers and in σ_e calculated by Mie theory using these $n(r)$. Jensen *et al.*, (1983) found that simultaneous measurements of $n(r)$ by colocated PMS spectrometers produced $n(r)$'s differing by a factor of 10 at all r's; σ_e's, obtained from these $n(r)$'s differed by a factor of 3 at λ's of 0.53, 1.06, 3.75, and 10.6 μm. Thus, errors of these magnitudes might be expected when comparing data taken by different PMS spectrometers. Some investigators have applied a correction to w obtained from $n(r)$ measured by spectrometers based on independent data (e.g., Slingo *et al.*, 1982b) while others have found w to be acceptable when compared with independent data (e.g., Herman and Curry, 1984).

3. Parameters derived from $n(r)$

The following parameters were derived from $n(r)$:

Number of droplets

$$N = \int n(r)dr \tag{1}$$

Mean droplet radius

$$\bar{r} = \frac{1}{N}\int rn(r)dr \tag{2}$$

Cross-section area

$$A = \pi \int r^2 n(r)dr \tag{3}$$

Liquid water content

$$w = \frac{4}{3}\pi D \int r^3 n(r)dr \tag{4}$$

Extinction coefficient

$$\sigma_e = \pi \int Q\left(\frac{2\pi r}{\lambda}, m\right) r^2 n(r)dr. \tag{5}$$

In (4), D is the density of water. In (5), Q is the total extinction cross section calculated from Mie-theory, normalized by the geometric cross section of the spherical particle and m is the complex index of refraction. The values of m used here are $(1.33 - i0)$, $(1.398 - i0.003)$ and $(1.270 - i0.052)$ for λ's of 0.53, 3.75 and 10.59 μm, respectively (Selby *et al.*, 1976). The units used here are: N (cm^{-3}), $n(r)$ (cm^{-3} μm^{-1}), $\bar{r}$ (μm), A (cm^2 m^{-3}), w (g m^{-3}) and σ_e (km^{-1}). Numerical integrations were performed over the range $0.23\ \mu\text{m} \leq r \leq 155\ \mu\text{m}$.

The three approximations to σ_e considered here are identified as σ_2, σ_3 and σ_4. The total extinction cross section Q in (5) may be approximated as a linear function of $2\pi r/\lambda$ when it is small and to be a constant equal to 2 when it is large. When $Q \approx 2$, (5) may be written

$$\sigma_2 = 2A. \tag{6}$$

Here σ_2 is commonly referred to as a small λ approximation to σ_e. When $Q \approx C2\pi r/\lambda$, (5) becomes

$$\sigma_e \approx \frac{2C\pi^2}{\lambda}\int r^3 n(r)dr. \tag{7}$$

After introducing w given by (4), (7) yields

$$\sigma_3 = \frac{3\pi C}{2D\lambda}w, \tag{8}$$

where σ_3 is commonly referred to as a large λ approximation to σ_e. Using the refractive indices given above, we note that the constant C is 0.73 and 0.48 for λ's of 3.75 and 10.59 μm, respectively. Thus, for these C's

$$\sigma_3 = 917w; \quad \lambda = 3.75\ \mu\text{m} \tag{8a}$$

$$\sigma_3 = 214w; \quad \lambda = 10.59\ \mu\text{m}. \tag{8b}$$

The units of σ_3 and w in (8a) and (8b) are km^{-1} and g m^{-3}, respectively.

The approximation σ_2 may be given in terms of the effective radius r_e, defined to be

$$r_e = \frac{\int r^3 n(r)dr}{\int r^2 n(r)dr}. \tag{9a}$$

Using (3) and (4), (9a) can be given as

$$r_e = \frac{3}{4D}\frac{w}{A}. \tag{9b}$$

According to (9b), σ_2 given by (6) can now be written as

$$\sigma_2 = \frac{3}{2D}\frac{w}{r_e}. \tag{10}$$

Since neither A nor r_e is generally available for stratus clouds, the small λ approximation σ_2 given by (6) or (10) is not presently useful, although (6) and (10) have been proposed as alternates to σ_e (Stephans, 1978b; Slingo and Schrecker, 1982). Although w is commonly determined in stratus clouds, σ_3 can be used only for sufficiently large λ. More general relationships between σ_e and w are needed for a wide range of λ's.

Log σ_e and log w have been found to be highly correlated (correlation coefficients > 0.95) over a large range of λ's. Accordingly, the following approximation to σ_e is made:

$$\sigma_4 = aw^b. \tag{11}$$

Gertler and Steele (1980) experimentally verified (11) for a λ of 10.6 μm for monodispersive and polydis-

persive droplets and Bruce *et al.*, (1980) experimentally verified (11) for λ's between 9.2 and 10.8 μm. Tonna and Valenti (1983) examined (11) using w obtained in 239 cases of fog for 74λ from 0.35 to 90 μm. These results indicate that (11) is applicable for many λ.

The constants a and b in (11) appear to vary with air mass because slightly different values of a and b have been reported for independent spectra observations (e.g., Pinnick *et al.*, 1979; Noonkester, 1981). Therefore, the disadvantage of using σ_4 to approximate σ_e is the need to know a and b for the air mass of interest. However, the use of improper values of a and b may produce smaller errors in estimations of σ_e than produced by σ_2 or σ_3. Table 1 gives values of a and b for the marine stratus data at λ of 0.53, 3.75 and 10.59 μm. These data are given according to the air mass and for the average of the two air masses.

Values of any of the foregoing parameters representing an entire 6.44 km path will be enclosed by the angle bracket $\langle(\ )\rangle$ implying an average over the path. Values without the angle bracket will represent data taken in the 429 m segments along the 6.44 km path.

4. Cloud base—a reference height

Marine stratus cloud layers have been modeled (e.g., Deardorff, 1980) and observed (e.g., Roach *et al.*, 1982; Slingo *et al.*, 1982b) to be well mixed and have a near dry adiabatic lapse rate of temperature below the cloud and a near moist adiabatic lapse rate in the cloud. The region where the relative humidity f is 100% separates the two distinctly different lapse rates. The most evident feature of a cloud is the reduced visibility above the saturation level where activated droplets are present. Thus, when comparing vertical changes in $n(r)$ or parameters derived from $n(r)$ in marine stratus layers, the saturation level is a natural, realistic, reference level as stressed by Betts (1983) for thermodynamic considerations.

TABLE 1. Values of a and b in Eq. (11) determined by regression analysis for the stratus cloud layer data. The correlation coefficients are greater than 0.98. Units are w (g m^{-3}), σ_4 (km^{-1}).

Air mass	λ (μm)	a	b
Marine	0.53	194	0.834
	3.75	308	0.950
	10.59	308	1.16
Continental	0.53	231	0.796
	3.75	351	0.949
	10.59	282	1.13
Average of marine and continental	0.53	212	0.812
	3.75	329	0.949
	10.59	294	1.14

Because the visibility gradually decreased as the airborne platform approached the stratus clouds from below and relative humidity was not available, a visual cloud base or saturation level could not be identified. Consequently, a reference level was established which was assumed to be near the saturation level. The data indicated that $n(r)$ contained activated droplets when $\langle w\rangle \geq 0.02$ g m^{-3}. Thus the reference level, defined to be cloud base and assumed to be near the saturation level, was assigned to be at the level where $\langle w\rangle = 0.02$ g m^{-3}. Figure 1 identifies the elevation of cloud base z_c on each measurement day according to this definition. The distance from z_c is defined to be z^*.

The cloud tops had minor billows and were sharply defined visually. The elevation of each cloud layer top z_t was assumed to be the average z along a horizontal run where the pilot attempted to fly in the minor billows about 50% of the time. The z_t are shown in Fig. 1.

5. Profiles of $\langle w\rangle$ and $\langle A\rangle$

When vertical profiles of w and A are available, vertical profiles of σ_2 [given by (6)], σ_3 and σ_4 can be constructed. Vertical profiles of $\langle w(z^*)\rangle$ and $\langle A(z^*)\rangle$ were constructed for the May (marine air mass) and August (continental air mass) data and for the average of the May and August data (equally weighted). These profiles are shown in Figs. 2 and 3. The regression equations for the average are given in Figs. 2b and 3b and the equations for the separate May and August data (Figs. 2a and 3a) are given in Table 2. The correlation coefficients associated with these equations are at least 0.97.

An unexplained large value of w was observed at one level just below cloud base on M29. This caused a positive perturbation of w from an exponential increase with elevation as shown in Fig. 2. This single data point was not used to obtain the regression equations for this region. The dashed line drawn through this region in Fig. 2 was assumed to represent the average $\langle w\rangle(z^*)$.

The profiles in Figs. 2 and 3 were subjectively drawn to provide continuous "best fit" curves to the data which closely approximate the regression equations. The regression equations produce small discontinuities at the terminating, common elevations.

6. Profiles of $\langle\sigma_e\rangle$

Values of σ_e were calculated from $\langle n(r)\rangle$ for each 2 min run shown in Fig. 1 at λ's of 0.53, 3.75 and 10.59 μm and were plotted as a function of the distance from cloud base z^*. (Data near the cloud top where σ_e began to decrease were not included because these data, apparently modified by entrainment, could not be used in averages for clouds of

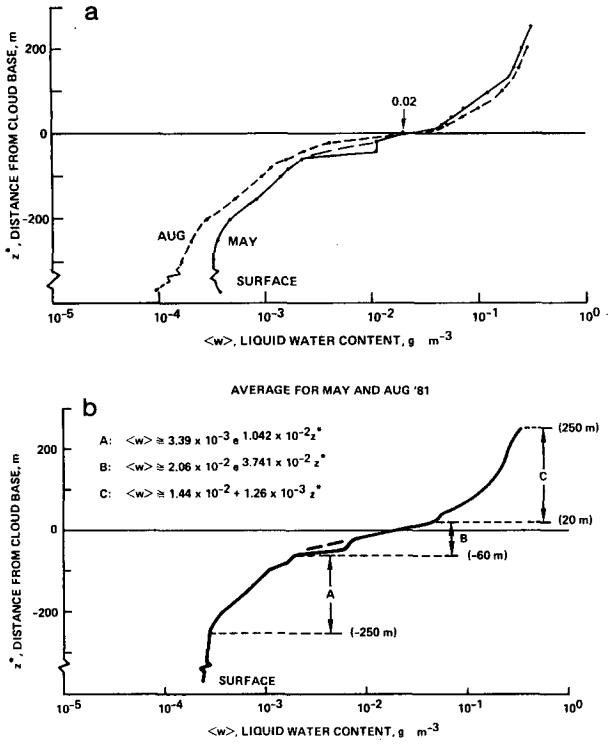

FIG. 2. Profiles of $\langle w \rangle$ as a function of the distance from cloud base ($\langle w \rangle = 0.02$ g m^{-3}). Dots on curves indicate elevations where averages were obtained. (a) May (modified marine) and August (aged continental) data; (b) the average of the May and August data (equally weighted).

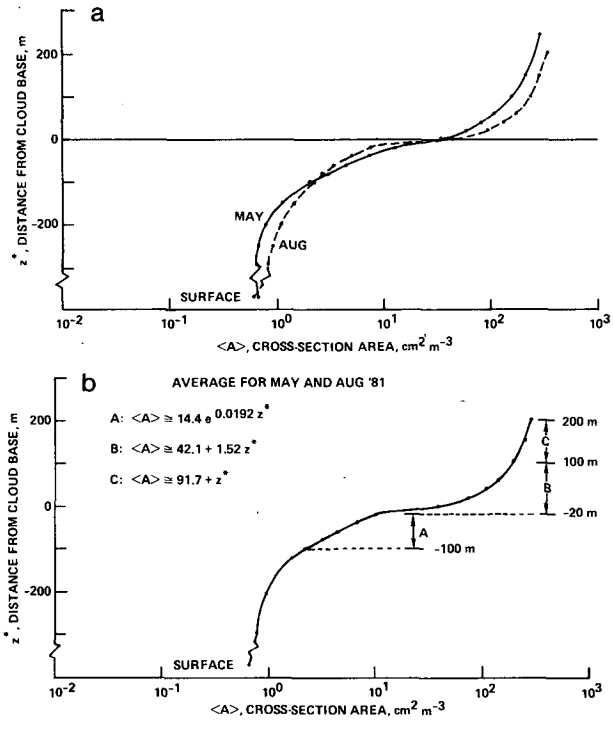

FIG. 3. As in Fig. 2, but of profile $\langle A \rangle$.

different depths.) Smooth curves were subjectively drawn through these data points to represent $\langle \sigma_e(z^*) \rangle$ for each day and λ. Values of $\langle \sigma_e \rangle$ were extracted from these curves at 16 selected z^* between 300 m below to 200 m above cloud base (also at $z^* = 250$ m for the May data). Figure 4 presents the resultant average $\langle \sigma_e(z^*) \rangle$ for the May and August data and the average for the combined May and August data at the selected elevations.

Equations, obtained by regression analyses, expressing $\langle \sigma_e \rangle$ as a function of z^* are given in Table 3. Figure 4 contains the regression equations for the average of the May and August data for the range -40 m $\leq z^* \leq 200$ m. The $\langle \sigma_e \rangle$ profiles displayed in Fig. 4 were subjectively drawn to provide continuous "best fit" curves to the data which closely approximate the regression equations. The regression equations given in Table 3 produce small discontinuities at the common elevations.

The profiles $\langle \sigma_e(z^*) \rangle$ shown in Fig. 4 were constructed from a limited number of curves (three for May and five for August). A statistical error analysis is not appropriate for the small sample size. Thus, figures showing profiles of $\langle \sigma_e(z^*) \rangle$ for each day and λ to illustrate the spread in the data would not portray or imply any reliability of the profiles.

7. Comparison of the extinction coefficients

Optical depths were used to compare the σ's. The optical depth τ is defined to be

TABLE 2. Regression equations for $\langle w(z^*) \rangle$ and $\langle A(z^*) \rangle$ where z^* is the distance from cloud base ($\langle w \rangle = 0.02$ g m^{-3}) for the May (modified marine) and August (aged continental) data. (Multiply $\langle A \rangle$ in cm^2 m^{-3} by 0.1 to get $\langle A \rangle$ in km^{-1}.)

Air mass	Elevation range z^* (m) Upper	Lower	Regression equation
			$\langle w \rangle$, (g m^{-3})
Marine	≥ -200	≤ -60	$0.0041 \exp(0.011z^*)$
(Fig. 2a)	> -60	≤ 20	$0.021 \exp(0.037z^*)$
	>20	≤ 250	$0.0093 + 0.0012z^*$
Continental	≥ 200	≤ -60	$0.0025 \exp(0.011z^*)$
(Fig. 2a)	> -60	<20	$0.017 \exp(0.048z^*)$
	≥ 20	≤ 200	$0.022 + 0.0013z^*$
			$\langle A \rangle$, (cm^2 m^{-3})
Marine	≥ -100	< -20	$19 \exp(0.022z^*)$
(Fig. 3a)	≥ -20	<100	$37 + 1.2z^*$
	≥ 100	≤ 250	$58 + 0.94z^*$
Continental	≥ -100	≤ -20	$10 \exp(0.016z^*)$
(Fig. 3a)	> -20	<100	$48 + 1.9z^*$
	≥ 100	≤ 200	$132 + z^*$

TABLE 3. Regression equations for $\langle\sigma_e\rangle$ as a function of distance from cloud base ($\langle w\rangle = 0.02$ g m^{-3}) for the May (modified marine) and August (aged continental) data and for the average (equally weighted) of the May and August data.

Air mass	λ (μm)	Elevation range z^* (m) Lower	Upper	Regression equation for $\langle\sigma_e\rangle$ (km^{-1})
Marine	0.53	≥ -250	< -100	$0.62 \exp(0.0058z^*)$
		≥ -100	≤ -40	$6.0 \exp(0.028z^*)$
		> -40	≤ 10	$8.9 \exp(0.038z^*)$
		> 10	≤ 250	$12 + 0.22z^*$
	3.75	≥ -250	< -100	$0.89 \exp(0.0084z^*)$
		≥ -100	≤ -40	$4.3 \exp(0.024z^*)$
		> -40	≤ 10	$10 \exp(0.047z^*)$
		> 10	≤ 250	$18 + 0.23z^*$
	10.59	≥ -250	< -100	$0.35 \exp(0.012z^*)$
		≥ -100	≤ -40	$1.3 \exp(0.023z^*)$
		> -40	≤ 10	$4.0 \exp(0.053z^*)$
		> 10	≤ 250	$2.6 + 0.27z^*$
Continental	0.53	≥ -250	< -100	$1.1 \exp(0.0069z^*)$
		≥ -100	< -40	$2.7 \exp(0.016z^*)$
		≥ -40	≤ 10	$10 \exp(0.050z^*)$
		> 10	≤ 200	$20 + 0.29z^*$
	3.75	≥ -250	≤ -100	$0.43 \exp(0.0062z^*)$
		> -100	≤ -40	$1.2 \exp(0.017z^*)$
		> -40	≤ 10	$11 \exp(0.073z^*)$
		> 10	≤ 200	$23 + 0.36z^*$
	10.59	≥ -250	≤ -100	$0.18 \exp(0.0096z^*)$
		> -100	≤ -40	$0.35 \exp(0.017z^*)$
		> -40	< 10	$2.7 \exp(0.071z^*)$
		≥ 10	≤ 200	$3.8 + 0.29z^*$
Average of marine and continental	0.53	≥ -250	≤ -100	$0.85 \exp(0.0061z^*)$
		> -100	< -40	$4.0 \exp(0.022z^*)$
		≥ -40	≤ 10	$9.7 \exp(0.044z^*)$
		> 10	≤ 200	$16 + 0.26z^*$
	3.75	≥ -250	≤ -100	$0.65 \exp(0.0075z^*)$
		> -100	≤ -40	$2.8 \exp(0.022z^*)$
		> -40	≤ 10	$11 \exp(0.057z^*)$
		> 10	≤ 200	$21 + 0.30z^*$
	10.59	≥ -250	< -100	$0.27 \exp(0.011z^*)$
		≥ -100	≤ -40	$0.81 \exp(0.021z^*)$
		> -40	≤ 10	$3.4 \exp(0.059z^*)$
		> 10	≤ 200	$3.3 + 0.28z^*$

$$\tau_i = \int_{z_2}^{z_1} \sigma_i(z^*)dz^*, \qquad (12)$$

where i is e, 2, 3 or 4 and z_1 and z_2 are the upper and lower values of z^* bounding the layer, respectively; σ_e, σ_2, σ_3 and σ_4 are given by (5), (6), (8) and (11), respectively; τ were calculated for the ranges -40 m $\leq z^* \leq 10$ m and 20 m $\leq z^* \leq 200$ m using the average of the May and August data. The regression equations for $\langle\sigma_e\rangle$, $\langle w\rangle$ and $\langle A\rangle$ were employed in (12). These τ_i are given in Table 4.

The values of τ_i in Table 4 reveal that σ_4, the power function of w, provides the best approximation to σ_e at all λ. The error in τ_4 is a minimum in the dense cloud region where all τ_i's are a maximum; τ_4 is within 3% of τ_e in the region 20 m $\leq z^* \leq$ 200 m and is within 13% of τ_e in the region -40 m $\leq z^* \leq 10$ m. The small λ approximation σ_2 provides a poor approximation to σ_e for a λ of 3.75 μm. The large λ approximation σ_3 provides a good estimate to σ_e only for a λ of 10.59 μm in the cloud.

8. Horizontal variations of σ_e

Convective cells are expected to be present in well mixed marine stratus layers (Deardorff, 1980; Caughey *et al.*, 1982) and to have horizontal scale sizes H appropriate for the mixed layer depth z_t and degree of instability (Fitzjarrald, 1978). Droplets, carried vertically in convective cells, may not be in equilibrium with the relative humidity so that droplet parameters measured along horizontal runs might reveal variations having the characteristic length H. Such nonequilibrium conditions might amplify H near z_c and z_t where droplet growth rates change rapidly when crossing the level of saturation.

Regardless of the cause of any irregularities present, they cannot be properly sampled if the characteristic $H \geq 6.44$ km, i.e., when trends are present. Also, any sources of variability created by instrumentation or sampling technique must be eliminated. The horizontal variability of σ_e on M29 and A18 was examined in detail.

a. Artificial variability

When the droplet count is sufficiently small along a horizontal run, the values of $n(r)$ determined for the fifteen 8 s (429 m) segments will be different even if the droplets are distributed homogeneously (equally spaced) along the run. These variations of $n(r)$ along a run are artificially created by the combined effects of relatively inadequate sampling volumes of the spectrometers and intermittent sampling of r-ranges by the ASSP-100 as discussed in Appendix A of Paper I. Artificial variability in $n(r)$ was concluded to be present in any sampling radius band Δr_i along a 6.44 km run if the droplet count within Δr_i was not at least 60 and 15 for the ASSP-100 and OAP-200, respectively.

The extinction coefficient σ_e given by (5), was numerically determined from the relation

$$\sigma_e = \pi \sum_{n=1}^{600} Q(r_n) r_n^2 n(r_n) \Delta r_n. \qquad (13)$$

There were 47 sampling radius bands Δr_i spanning the radius range 0.23 μm $\leq r \leq$ 155 μm. The 600 radius bands Δr_n in (13) were created by applying a cubic spline to interpolate values of $n(r)$ between midpoint r_i of adjacent Δr_i. To determine regions of $n(r)$ creating artificial variability in σ_e, σ_e given by

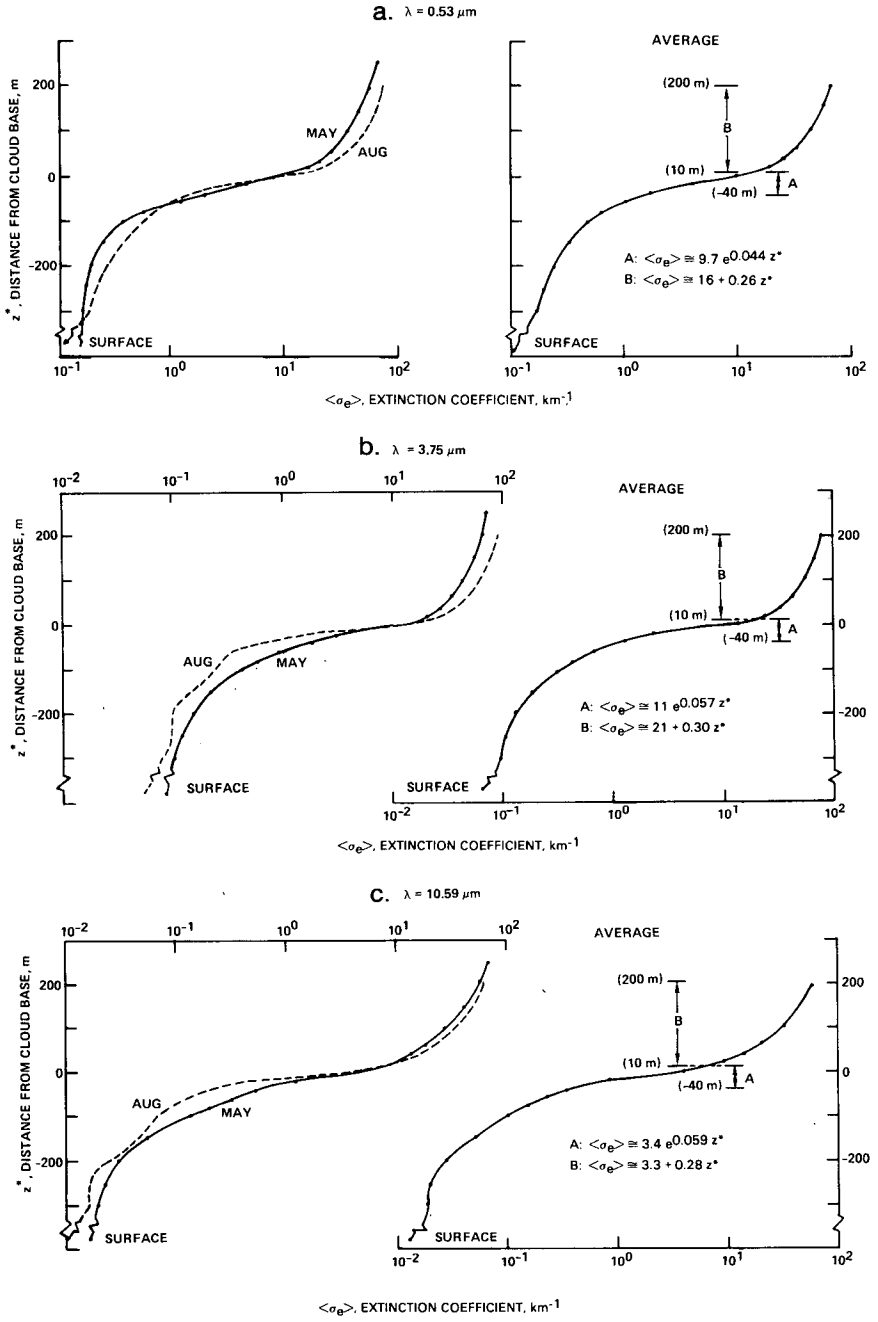

FIG. 4. Profiles of the optical extinction coefficient $\langle \sigma_e \rangle$ by (5) (droplets only) as a function of distance from the cloud base ($\langle w \rangle = 0.02$ g m^{-3}) for the May (modified marine) and August (aged continental) data and for the average of the May and August data (equally weighted). Dots on curves indicate elevations where averages were obtained. (a) $\lambda = 0.53$ μm; (b) $\lambda = 3.75$ μm; (c) $\lambda = 10.59$ μm.

(13) was approximated by substituting a summation over the $47\Delta r_i$'s for the $600\Delta r_n$'s. The horizontal variability of σ_e on M29 and A18 was considered to be artificial when a region of $\langle n(r) \rangle$ contributed an appreciable amount ($\geq$20%) to $\langle \sigma_e \rangle$ and the $\langle n(r_i) \rangle$'s in this region were determined by droplet counts less than the minimum (60 and 15 for the ASSP-100 and OAP-200, respectively). Levels containing artificial variations in σ_e included the levels above cloud top and at z^*'s ≤ -40 m for λ of 3.75 and 10.59 μm. Although artificial variations in σ_e were absent at all levels for $\lambda = 0.53$ μm on both days, the horizontal

TABLE 4. Optical depths τ for vertical transmissions at three λ through two regions of the average (equally weighted) of the May and August data. The extinction is by droplets only. The subscript of the τ corresponds to the subscript of the associated σ [use (5), (6), (8) and (11) for $i = e$, 2, 3 and 4, respectively].

Optical depth τ_i	Wavelength λ (μm) 0.53	3.75	10.59
	$20 \text{ m} \leq z^* \leq 200 \text{ m}$		
τ_e	8.0	9.7	6.1
τ_2	7.0	7.0	—
τ_3	—	25.2	5.9
τ_4	8.2	9.9	6.3
	$-40 \text{ m} \leq z^* \leq 10 \text{ m}$		
τ_e	0.30	0.32	0.10
τ_2	0.19	0.19	—
τ_3	—	0.62	0.15
τ_4	0.32	0.28	0.11

variability was examined only at levels where at least two of the three σ_e were free of artificial variations. These levels are shown in Fig. 5.

b. Scale size

Values of horizontal variability cannot be considered representative if the magnitude of the σ_e steadily increases or decreases along a level. That is, if the characteristic scale size H is approximately equal to or greater than 6.44 km, trends are present and must be excluded in the analysis.

A simple method was used to estimate H along flight levels shown in Fig. 5 where artificial variability was absent on M29 and A18. The number α of the positive and negative deviations of each σ_e from its mean over each flight level was obtained. For example, α would be 2 if values of σ_e approximated a sine wave about its mean along a run and H would be 6.44 km. That is, $H \approx 6.44(0.5\alpha)^{-1}$ km. The average α was determined for the three σ_e (two σ_e at lowest level on A18). Figure 5 presents the resulting H's.

Significant trends were assumed to be present at levels where $H > 6.4$ km; these H's are circled in Fig. 5. The average H of the remaining H's was 2.9 and 3.1 km on M29 and A18, respectively, giving an average H of 3.0 km. This average H is essentially identical to the average of 2.9 km found for N, w and $\bar{r}$ at these levels on the same two days (Paper I). Thus, artificial variability and trends were assumed to be absent at all levels in Fig. 5 except at levels where H is circled. The horizontal variability at the remaining levels was assumed to be representative of M29 and A18.

Although the runs were essentially vertically spaced in the same vertical plane, the beginning (or ending) points of each run had slightly different geographic locations and the runs were separated in time during which the vertical features of the stratus layer may have changed. This prevented the determination of any vertical continuity of H. The average H of 3 km could have been in phase over the entire cloud depth. If so, the horizontal variation of optical properties for propagation along vertical paths could have been determined for this scale size.

c. Magnitude of horizontal variability

The relative variability was defined to be given by the fraction $s_{\sigma_e}/\langle\sigma_e\rangle$ where s_{σ_e} is the standard deviation

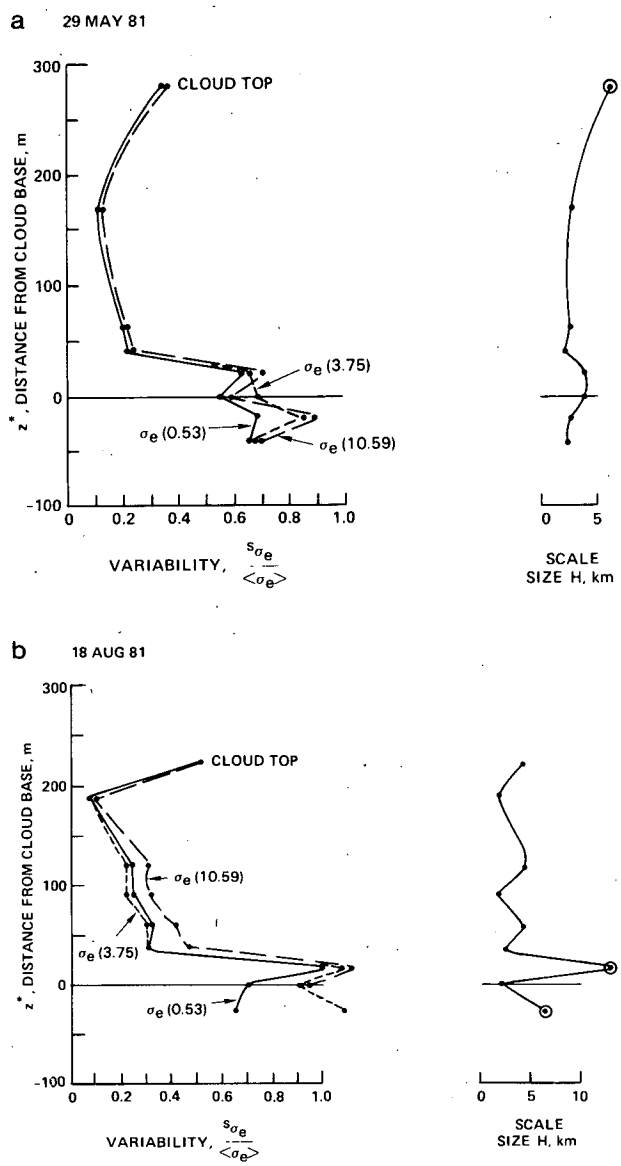

FIG. 5. Vertical profiles of the relative horizontal variability of σ_e and the horizontal scale size H. Dots are at the sampling elevations. (a) 29 May 1981 (M29); (b) 18 August 1981 (A18).

of the $15\sigma_e$ along a run. Figure 5 presents the relative horizontal variability of σ_e in the elevation range $-38 \text{ m} \leq z^* \leq z_t$ for M29 and $-27 \text{ m} \leq z^* \leq z_t$ for A18. Within these ranges, only σ_e ($\lambda = 10.59$ μm) at $z^* = -27$ m on A18 contained artificial variations; the corresponding value of $s_{\sigma_e}/\langle\sigma_e\rangle$ was not entered in Fig. 5.

The relative variabilities $s_{\sigma_e}/\langle\sigma_e\rangle$ in Fig. 5 have primary maximums near cloud base, secondary maximums at cloud top and minimums in the middle to upper regions of the clouds. The location of these maximum/minimum values correspond to the location of the maximum/minimum values of variability of N, w and $\bar{r}$ (Paper I) on these days. Vertical, turbulent mixing (scale size $H \approx 3$ km) is believed to be the most likely cause of the horizontal variability because the average gradient of the relative humidity f, the principal factor controlling $n(r)$, is greater in the vertical plane than in the horizontal plane. Vertical motion of droplets across the level where $f \approx 100\%$ near cloud top and base is expected to create large changes in $n(r)$ (nonequilibrium conditions) compared to changes associated with vertical motion deeper within the cloud.

The relative variability is about 30% in the upper regions of the clouds where the σ_e are a maximum. Accordingly, this variability would essentially control the variability of the τ_e for the cloud layers. Simultaneous measurements at several levels near cloud top appear necessary to establish the vertical phase relations of σ_e.

9. Discussion

a. Cloud base

A level representing the saturation level provides a realistic one for comparing vertical variations of droplet parameters in the stratus layers from one day to the next. In-cloud droplet parameters are a function of cloud thickness so that the cloud top elevation (inversion base) would not be an appropriate reference level. The saturation level is a critical level for vertically moving droplets relative to droplet growth characteristics. The elevation where w was about 0.02 g m^{-3} appeared to provide an estimate of the saturation level relative to changes in $n(r)$ for all measurement days. The droplet parameters changed from an exponential to a linear dependence on elevation near the level where $w = 0.02$ g m^{-3} according to the regression analyses. The capability of the droplet model by Fitzgerald (1975) (see Paper I) to approximate w below the defined cloud base provided good reason to accept a value of w of 0.02 g m^{-3} as near the saturation level.

b. Approximation σ_4

There appears to be no ideal approximation to the optical extinction coefficient σ_e expressed as functions of parameters derived from $n(r)$. As expressed by (5), σ_e involves integration over r of the product of three factors, all functions of r and one also a function of λ. Because $n(r)$ is the critical function in (5) for a selected λ and refractive index, σ_e varies with the shape characteristics of $n(r)$ over the range of integration. Correctly applied, the small and large λ approximations, σ_2 and σ_3, respectively, are restricted to a limited range of r which is usually insufficient because droplets, not in the radius range appropriate for the approximations, often contribute an appreciable fraction to σ_e. Accordingly, the utility of using σ_2 and σ_3 as approximations to σ_e in the stratus clouds is concluded to be unacceptable as demonstrated by the differences $\tau_e - \tau_2$ and $\tau_e - \tau_3$ (Table 4).

Because w alone cannot specify a unique $n(r)$, it is surprising that σ_4, a power function of w, closely approximates σ_e as indicated by the relatively small values of $\tau_e - \tau_4$ (Table 4).

The magnitude of $n(r)$ at any r depends on the type and number-size distribution of the droplet nuclei for a selected relative humidity f (Fitzgerald, 1974, 1975; Hudson, 1980, 1983). Changes in $n(r)$ will depend on the nuclei set involved as f changes. Thus, values of a and b in σ_4 will vary as the nuclei-set, or roughly, the air mass, varies in response to the change in the distribution of $d\sigma_e/dr$ and dw/dr over $n(r)$. Accordingly, the selection of a and b must be appropriate for the air mass embedding the stratus cloud layer. When a and b are suitable for the air mass being considered, σ_4 should provide a good approximation to σ_e. The use of an average a and b is expected to reveal that σ_4 is superior to σ_2 and σ_3 as an approximation to σ_e for most stratus cloud layers.

c. Sampling distance

If the source of the horizontal variability in σ_e is atmospheric turbulence, then the approximate horizontal distance L required to obtain an average $\langle\sigma_e\rangle$ with an acceptable error ϵ in the relative variability is (Lumley and Panofsky, 1964):

$$L \approx 2l\left(\frac{s_{\sigma_e}/\langle\sigma_e\rangle}{\epsilon}\right)^2 \tag{14}$$

where l is an integral scale length. The sample variability is used as an estimate of the population variability $s_{\sigma_e}/\langle\sigma_e\rangle$ and l scales as the depth of the mixed layer z_t.

The vertical profiles of the relative variability $s_{\sigma_e}/\langle\sigma_e\rangle$ in the elevation range shown in Fig. 5 are almost identical to $s_w/\langle w\rangle$ presented in Paper I which might be expected because the σ_e's are highly correlated with w. Thus, the L values for the σ_e are approximately equal to the L's of the $\langle w\rangle$'s when assuming the same relative error ϵ. The average L for $\langle w\rangle$ was 36 km on M29 and A18 when ϵ was 0.1

(10%). A 36 km averaging distance is 5.6 times greater than the sample distance of 6.44 km. If 36 km horizontal runs were used, about six hours would be required to sample the stratus layer when measuring at 13 to 15 levels. Even if the layer were not changing with time, the 36 km runs would likely span mesoscale changes, so that unacceptable trends would be present. Techniques to decrease L for a fixed ϵ in such layers do not appear to be available.

10. Conclusions

This report has presented vertical profiles of single scatter extinction coefficients $\langle\sigma_e\rangle$ by droplets at selected wavelengths (λ = 0.53, 3.75 and 10.59 μm) for stratus cloud layers concluded to have formed in either modified marine or continental air masses. These profiles of $\langle\sigma_e\rangle$, determined from Mie-theory calculations, extended from 200 m above to 250 m below the cloud base. The cloud base was defined to be at the elevation where the liquid water content $\langle w\rangle$ was 0.02 g m^{-3}. Profiles of the three $\langle\sigma_e\rangle$ were also presented for the average of the two air masses. These data are thought to be the first to show continuous profiles of $\langle\sigma_e\rangle$ over a 450 m depth for marine stratus cloud layers using internally consistent data.

Approximations to $\langle\sigma_e\rangle$, given as a linear function of the cross section area $\langle A\rangle(\sigma_2)$ and of $\langle w\rangle(\sigma_3)$ and as a power function of $\langle w\rangle(\sigma_4)$, were examined to determine their capability to specify $\langle\sigma_e\rangle$ in the average stratus cloud. Differences between the optical depths τ resulting from the approximations ($\langle\sigma_2\rangle$, $\langle\sigma_3\rangle$ and $\langle\sigma_4\rangle$) and τ resulting from $\langle\sigma_e\rangle$ in the cloud and near the cloud base were compared to select the best approximation to $\langle\sigma_e\rangle$. $\langle\sigma_4\rangle$ was found to be a superior approximation to $\langle\sigma_e\rangle$. The constants in the power function $\langle\sigma_4\rangle$ depend on the shape characteristic of $\langle n(r)\rangle$. Thus, the power function of $\langle w\rangle$ selected for a marine stratus cloud layer must be appropriate for the air mass and other factors (e.g., turbulent mixing) controlling the shape of $n(r)$.

Profiles of $\langle A\rangle$ and $\langle w\rangle$ were also presented for the two air masses and for the average air mass. These profiles can be used if good approximations to $\langle\sigma_e\rangle$ involving functions of $\langle A\rangle$ and $\langle w\rangle$ are developed.

The relative horizontal variability of σ_e was examined for two representative days. The variability was a maximum near the cloud top and base and a minimum in the upper regions of the cloud. The horizontal variations in σ_e were highly correlated at an average scale size estimated to be 3 km. The vertical continuity (phase relationship) of the horizontal variability could not be determined.

The horizontal averaging distance L required to obtain a value of $\langle\sigma_e\rangle$ with a relative accuracy of 10% was estimated to be about 36 km in two representative stratus layers. Methods of obtaining $\langle\sigma_e\rangle$ with relative accuracies approaching a few percent from $\langle n(r)\rangle$ over smaller horizontal measuring distances appear necessary to avoid variability created by temporal and mesoscale changes in marine stratus cloud layers.

The profiles of $\langle\sigma_e\rangle$ and the comparison of σ_e with their approximations should provide guidance in the development of parameterization schemes describing the influence of marine stratus clouds on the atmospheric radiation balance.

Acknowledgments. The acquisition of the $n(r)$ data was sponsored by the Naval Air Systems Command (Program Element 61153N; Project WR03302). The analysis of the optical extinction coefficient data was sponsored by the Naval Air Systems Command (Program Element 62759N; Project F59551). The author is indebted to D. R. Jensen who diligently acquired excellent data and to B. L. Thomason who processed the data with great care.

REFERENCES

Baumgardner, D., and J. E. Dye, 1983: The 1982 particle measurement symposium, 4–7 May 1982, Boulder, Colorado. *Bull. Am. Meteor. Soc.*, **64,** 366–370.

Betts, A. K., 1983: Thermodynamics of mixed layer stratocumulus layers: Saturation point budgets. *J. Atmos. Sci.*, **40,** 2655–6670.

Bruce, D., C. W. Bruce, Y. P. Yee, L. Cahenzli and H. Burket, 1980: Experimentally determined relationship between extinction coefficients and liquid water content. *Appl. Opt.*, **19,** 3355–3360.

Caughey, S. J., B. A. Crease and W. T. Roach, 1982: A field study of nocturnal stratocumulus: II. Turbulence structure and entrainment. *Quart. J. Roy. Meteor. Soc.*, **108,** 125–144.

Davies, R., 1978: The effect of finite geometry on the three-dimensional transfer of solar irradiance in clouds. *J. Atmos. Sci.*, **35,** 1712–1725.

Deardorff, J. W., 1980: Stratocumulus-capped mixed layers derived from a three-dimensional model. *Bound.-Layer Meteor.*, **18,** 495–527.

Fitzgerald, J. W., 1974: Effect of aerosol composition on cloud droplet size distribution: A numerical study. *J. Atmos. Sci.*, **31,** 1358–1367.

——, 1975: Approximation formulas for the equilibrium size of an aerosol particle as a function of its dry size and composition and the ambient relative humidity. *J. Appl. Meteor.*, **14,** 1044–1049.

Fitzjarrald, D. E., 1978: Horizontal scales of motion in atmospheric free convection observed during the GATE experiment. *J. Appl. Meteor.*, **17,** 213–221.

Gertler, A. W., and R. L. Steele, 1980: Experimental verification of the linear relationship between IR extinction and liquid water content of clouds. *J. Appl. Meteor.*, **19,** 1314–1317.

Herman, G. F., Man-Li C. Wu and W. T. Johnson, 1980: The effect of clouds on the earth's solar and infrared radiation budgets. *J. Atmos. Sci.*, **37,** 1251–1261.

——, and J. A. Curry, 1984: Observational and theoretical studies of solar radiation in Arctic stratus clouds. *J. Climate and Appl., Meteor.*, **25,** 5–24.

Hidy, G. M., P. K. Mueller, H. H. Wang, J. Karney, S. Twiss, M. Imada and A. Alcocer, 1974: Observations of aerosols over Southern California coastal waters. *J. Appl. Meteor.*, **13,** 96–107.

Hudson, J. G., 1980: Relationship between fog condensation nuclei and fog microstructure. *J. Atmos. Sci.*, **37,** 1854–1867.

——, 1983: Effects of CCN concentrations on stratus clouds. *J. Atmos. Sci.*, **40,** 480–485.

Jensen, D. R., R. Jeck, G. Trusty and G. Schacher, 1983: Intercomparison of PMS particle size spectrometers. *Optical Eng.*, **22,** 746–752.

Lumley, J. L., and H. A. Panofsky, 1964: *The Structure of Atmospheric Turbulence,* Wiley and Sons, 239 pp.

Neiburger, M., and C. W. Chien, 1960: Computations of the growth of cloud drops by condensation using an electronic digital computer. *Physics of Precipitation.*, Geophys. Monograph No. 5, Amer. Geophys. Union, 191–210, (NAS-NRC Pub. 746).

Noonkester, V. R., 1981: Extinction coefficients calculated from aerosol spectra measured in a convective layer with stratus. *Appl. Opt.*, **20,** 1275–1277.

——, 1984: Droplet spectra observed in marine stratus cloud layers. *J. Atmos. Sci.*, **41,** 829–845.

Pinnick, R. G., S. G. Jennings, P. Chylek and H. J. Auvermann, 1979: Verification of a linear relation between IR extinction, absorption and liquid water content of fogs. *J. Atmos. Sci.*, **36,** 1577–1586.

Roach, W. T., R. Brown, S. J. Caughey, B. A. Crease and A. Slingo, 1982: A field study of nocturnal stratocumulus: I. Mean structure and budgets. *Quart. J. Roy. Meteor. Soc.*, **108,** 103–123.

Selby, J. E. A., E. P. Shettle and R. A. McClatchey, 1976: Atmospheric Transmittance from 0.25 to 28.5 μm: Supplement LOWTRAN 3B (1976). Air Force Geophys. Lab., Hanscom AFB, MA, Report AFGL-TR-76-0258, 79 pp.

Slingo, A., S. Nicholls and J. Schmetz, 1982a: Aircraft observations of marine stratocumulus during JASIN. *Quart. J. Roy. Meteor. Soc.*, **108,** 833–856.

——, R. Brown and C. L. Wrench, 1982b: A field study of nocturnal stratocumulus; III. High resolution radiative and microphysical observations. *Quart. J. Roy. Meteor. Soc.*, **108,** 145–165.

——, and H. M. Schrecker, 1982: On the shortwave radiative properties of stratiform water clouds. *Quart. J. Roy. Meteor. Soc.*, **108,** 407–426.

Stephens, G. L., 1978a: Radiation profiles in extended water clouds. I: Theory. *J. Atmos. Sci.*, **35,** 2111–2122.

——, 1978b: Radiation profiles in extended water clouds, II. Parameterization schemes. *J. Atmos. Sci.*, **35,** 2123–2132.

Tonna, G., and C. Valenti, 1983: Optical attenuation coefficients and liquid water content relationship in fog, at seventy-four wavelengths from 0.35 to 90 μm. *Atmos. Environ.*, **17,** 2075–2080.